European Journal of Pharmaceutical Sciences 171 (2022) 106133

Contents lists available at ScienceDirect

European Journal of Pharmaceutical Sciences

journal homepage: www.elsevier.com/locate/ejps

Improved solubility of lornoxicam by inclusion into SBA-15: Comparison of loading methods

Adrianna Dadej [a,*], Aneta Woźniak-Braszak [b], Paweł Bilski [c,d], Hanna Piotrowska-Kempisty [e], Małgorzata Józkowiak [e], Anna Pawełczyk [f], Daniela Dadej [g], Dominika Łażewska [a], Anna Jelińska [a]

[a] Poznan University of Medical Sciences, Faculty of Pharmacy, Chair and Department of Pharmaceutical Chemistry, Grunwaldzka 6, 60-780, Poznań, Poland
[b] Adam Mickiewicz University, Faculty of Physics, Functional Materials Physics Division, Uniwersytetu Poznańskiego 2, 61-614, Poznań, Poland
[c] Adam Mickiewicz University, Faculty of Physics, Medical Physics and Radiospectroscopy Division, Uniwersytetu Poznańskiego 2, 61-614, Poznań, Poland
[d] Frank Laboratory of Neutron Physics, Joint Institute for Nuclear Research, 141980, Dubna, Russian Federation
[e] Poznan University of Medical Sciences, Faculty of Pharmacy, Chair and Department of Toxicology, Dojazd 30, 60-631, Poznań, Poland
[f] Poznan University of Medical Sciences, Faculty of Pharmacy, Chair and Department of Organic Chemistry, Grunwaldzka 6, 60-780, Poznań
[g] Poznan University of Medical Sciences, Faculty of Medicine, Chair and Department of Endocrinology, Metabolism and Internal Diseases, Przybyszewskiego 49, 60-355, Poznań, Poland

ARTICLE INFO

Keywords:
SBA-15
Mesoporous silica
Drug delivery system
Dissolution rate
Lornoxicam
Physicochemical techniques

ABSTRACT

An increasing proportion of new medicinal substances are poorly soluble in water. Adsorption on mesoporous silicas increases their bioavailability when administered orally. Loading method determines adsorption either on the surface in crystalline state or inside the mesopores in amorphus form. The aim of this study was to compare two methods (adsorption equilibrium and solvent evaporation) of lornoxicam adsorption on SBA-15 and APTES-modified SBA-15 in terms of drug adsorption site. Additionally, we investigated the drug release profiles at different pH and cytotoxicity of the analysed mesoporous materials. The materials were characterized by a number of physicochemical techniques including X-ray diffraction, nitrogen adsorption/desorption techniques, differential scanning calorimetry, thermogravimetric analysis, scanning and transmission electron microscopy, infrared spectroscopy and ^{1}H NMR. Lornoxicam was loaded on the studied materials and released in the media (HCl pH 1.2, phosphate buffers pH 6.8 and 7.4). The cytotoxicity assays of APTES-modified SBA-15 were performed on CaCo-2 human colon cancer cell line. We proved that adsorption equilibrium method is a more advantageous method of loading. It ensures drug adsorption in an amorphous state inside the mesopores. The solvent evaporation method, despite a greater amount of loaded drug, results in drug adsorption in a crystalline state on the silica surface. In drug release studies a greater amount of lornoxicam is released from modified materials compared to crystalline lornoxicam. Cytotoxicity study proved the safety of APTES-modified silica. We concluded that APTES-modified SBA-15 is applicable as an effective and non-toxic carrier for the poorly soluble drug lornoxicam. The adsorption equilibrium method should be the preferred loading method. It enables the adsorption of sparingly soluble substances inside the mesoproes and enhances bioavailability of oral pharmaceutical forms.

1. Introduction

In recent years, silica mesoporous materials have aroused widespread interest from the scientific community. Since Mobil Oil Company first synthesized mesoporous silicas in 1992, the number of scientific reports focusing on this material have increased continuously. Numerous modifications of the synthesis' conditions, as well as the use of various structurally ordering agents allowed to obtain a product with the desired properties (Chaudhary and Sharma, 2017).

Mesoporous silicas are characterized by a large specific surface area with the possibility of its modification (Almáši et al., 2020), a large pore volume, tunable particle size and high thermal and chemical stability

* Corresponding author: Adrianna Dadej, Poznan University of Medical Sciences, Faculty of Pharmacy, Chair and Department of Pharmaceutical Chemistry, Grunwaldzka 6, 60-780, Poznań, Poland.
E-mail address: dadej.adrianna@gmail.com (A. Dadej).

https://doi.org/10.1016/j.ejps.2022.106133
Received 21 August 2021; Received in revised form 9 November 2021; Accepted 19 January 2022
Available online 21 January 2022

(Moritz and Geszke-Moritz, 2015). Moreover, they show low toxicity and high biocompatibility (Zhou et al., 2018). In the context of planned research they improve the dissolution rate of sparingly soluble substances via maintaining the amorphous state and preventing transition to a crystalline state (Biswas, 2017). The mesoporous silica is characterised by a high surface free energy resulting from a large specific surface area. This allows the transition of the system to a state of lower free energy after the drug loading, resulting in the conversion of adsorbed molecules into a physically stable amorphous state (Brus et al., 2017).

The unique properties of silicas have allowed their application in many fields of science and industry. They are used in catalysis (Perego and Millini, 2013), molecules' separation (Wan et al., 2009) or as sensor devices (Anu Prathap et al., 2012). In pharmacy, they serve as drug delivery systems (Almáši et al., 2020), enabling modification of the drug release site (Sarkar et al., 2016), slowing the release process (Kim et al., 2018) or improving bioavailability by increasing the solubility of active substances (Abd-Elrahman et al., 2016; Esperanza Adrover et al., 2020).

Improvement of dissolution rate is important for the design of new pharmaceutical forms as most of new drugs are characterized by poor water-solubility and thus reduced bioavailability (Abd-Elrahman et al., 2016). It is then necessary to increase the drug dose to achieve a therapeutic concentration, resulting in the increased risk of side effects. The aforementioned active substances with low water solubility belong to class II and IV of the BCS classification system (Biopharmaceutics Classification System).

Lornoxicam (LOX) is a drug representing class II with low solubility and high permeability through biological membranes (Nijhawan et al., 2014). It belongs to the group of non-steroidal anti-inflammatory drugs that exert analgesic, anti-inflammatory and antipyretic effects. It is widely used to relieve pain in the postoperative period and in the course of rheumatoid arthritis (Byrav et al., 2009). Improving the solubility of lornoxicam would increase its bioavailability and allow dose reduction, thus decreasing the risk of side effects.

Several methods to increase the dissolution rate of lornoxicam were proposed so far including the formation of complexes with cyclodextrins (Hamza and Aburahma, 2009; Moutasim et al., 2017), solid dispersions (Tawfeek et al., 2014), emulsions (Li et al., 2015) and the formation of cocrystals (Nijhawan et al., 2014). The analysis of lornoxicam adsorption on unmodified mesoporous silica SBA-15 was also investigated (Vishal, 2015).

The aim of this study was to analyse lornoxicam adsorption on two types of mesoporous silica: SBA-15 and SBA-15 modified with APTES and to compare two methods: adsorption equilibrium and solvent evaporation technique, in terms of process efficiency and the adsorption site of lornoxicam on the material. We also analysed the release profiles of the substance in different media at various pH, which we compared with the dissolution profile of the drug. In addition, we characterized the obtained silicas by X-ray diffraction (XRD), differential scanning calorimetry (DSC), infrared spectroscopy (FT-IR), ^{1}H NMR, low-temperature nitrogen sorption, scanning and transmission electron microscopy (SEM and TEM). Moreover, we performed cytotoxicity assays of APTES-modified SBA-15 before and after lornoxicam loading.

2. Material and methods

2.1. Chemicals and materials

Tetraethyl orthosilicate (TEOS) (≥99.0%), Pluronic®P-123, (3-aminopropyl) triethoxysilane (APTES) (99%), hydrochloric acid (purum p.a. ≥32.0%), anhydrous toluene (99.8%), sodium dodecyl sulfate (≥99.0%) were purchased from Sigma–Aldrich. Chloroform (p.a. ≥98.5%), potassium dihydrogenphosphate (pure p.a.), sodium chloride (pure p.a.), sodium hydroxide 0.1 mol/l(0.1 N) analytical weighed amount liquid, analytical weight of hydrochloric acid 0.1 mol/l(0.1 N) were supplied from Avantor Performance Materials Poland. Dimethyl sulfoxide (pure p.a. ≥99.7%) was obtained from Chempur. Lornoxicam (>98%) was purchased from Tokyo Chemical Industry CO.

2.2. Synthesis of mesoporous materials

The synthesis of SBA-15 mesoporous silica was carried out in accordance with the methodology described by Zhao et al. (Zhao et al., 1998) with modifications. The synthesis proceeded at 35 °C as follows: 24.0 g of poly (ethylene glycol) and poly (propylene glycol) block copolymer (Pluronic P123) was dissolved in 900 ml of aqueous HCl (1.6 M). Next, 51.0 g of tetraethylorthosilicate (TEOS) was added into the solution and magnetically stirred at 35 °C for 20 h. Subsequently, the mixture was aged at 110 °C for 24 h. Further, the suspension was filtered and washed with distilled water. Finally, the precipitate was air dried and the resulting silicas were calcined at 500 °C for 6 h (heating rate 1 °C/min).

2.3. Functionalization of mesoporous matrices with organic groups

APTES ((3-aminopropyl) triethoxysilane) functionalized mesoporous silica was obtained by grafting method. First, the silica was dried at 110 °C for 24 h. Next, 3.0 g of silica was mixed with 50 ml of APTES solution in toluene (0.10 mol /l). Then, the mixture was heated at 100 °C for 24 h in a borosilicate bottle with a PTFE stopper. The resulting solid was filtered and rinsed initially with anhydrous toluene (5 × 75 ml) and subsequently with chloroform (5 × 75 ml). The final product was dried at 40 °C for 3 h and then at 80 °C for 24 h to remove the residual organic solvent. The APTES-modified material was designated as SBA-15-pr-NH_2.

2.4. Lornoxicam adsorption studies

Adsorption studies were conducted using two methods.

2.4.1. Adsorption equilibrium method

Adsorption studies of LOX involved preparation of a 3.0 mg/ml LOX solution in DMSO and combining 5.0 ml of prepared solution with 50.0 mg of SBA-15-pr-NH_2 silica. The obtained mixture was then stirred for 48 h at 25 °C to achieve equilibrium adsorption state. The suspension was further centrifuged at 6000 rpm for 15 min. The precipitate was dried at 50 °C for 14 days. The resulting material with the adsorbed substance was designated as SBA-15-pr-NH_2:LOX.

The amount of non-adsorbed LOX in the diluted supernatant was evaluated using UV/VIS LAMBDA 20 Perkin Elmer spectrophotometer at 396 nm. The amount of adsorbed LOX was calculated as the difference in the solution concentration before and after adsorption.

2.4.2. Solvent evaporation technique

Each sample containing 50.0 mg of SBA-15 or SBA-15-pr-NH_2 silica was mixed with 5.0 ml of a 3.0 mg/ml LOX solution in DMSO. The solvent was then evaporated until a dry powder was obtained. The samples were designated as eSBA-15:LOX and eSBA-15-pr-NH_2:LOX respectively.

The amount of adsorbed LOX was determined by spectrophotometric method after releasing the adsorbed LOX in DMSO.

The drug loading efficiency for both methods was calculated according to the following formula (Pardhi et al., 2017; Wang et al., 2014): *Drug loading efficiency [%] = Weight of LOX in the sample [mg]/ Weight of carrier in the sample [mg]*100%*.

2.5. Characterization methods

2.5.1. Powder X-ray diffraction (XRD)

Small-angle powder X-ray diffraction patterns were obtained with Bruker D8 Advance in the range from of 0.6 to 8.0° with a 0.02° step width associated with a step time of 1–2 s. Wide-angle powder X-ray

diffraction patterns were obtained with Bruker D2 Phaser in the range from of 5.0 to 45.0° with a 0.02° step width associated with a step time of 1–2 s.

2.5.2. Nitrogen adsorption/desorption

Nitrogen adsorption/desorption isotherms were measured at −196 °C with Autosorb iQ analyser (Quantachrome Instruments). Prior to the analysis, pure silica samples were degassed in a vacuum at 100 °C for 24 h and samples with adsorbed LOX at room temperature for 24 h. The specific surface area was determined by BET (Brunauer-Emmett-Teller) isotherm. The pore volume, diameter and size distribution were obtained from the desorption branch of the isotherm according to BJH (Barret-Joyner-Halenda) method.

2.5.3. Differential scanning calorimetry (DSC)

Differential scanning calorimetry measurements were performed using DSC 214 Polyma Netzsch in nitrogen atmosphere (30 ml/min). All samples (~5 mg) were heated from 25 to 250 °C with scanning rate of 5 °C/min.

2.5.4. Thermogravimetric analysis (TGA)

Thermogravimetric measurements were carried out with TG 209 F3 Tarsus Netzsch using nitrogen as a carrier gas (30 ml/min). The samples (~3 mg) were heated up to 600 °C with a heating rate of 10 °C/min.

2.5.5. Transmission and scanning electron microscopy (TEM and SEM)

TEM images were taken by JOEL JEM 1200 EX electron microscope operated at 80 kV and SEM images were obtained on Zeiss EVO-40 electron microscope.

2.5.6. Fourier transformed infrared spectroscopy (FTIR) and UV–Vis spectrophotometry

The FTIR spectra were recorded on Bruker FTIR IFS 66/s spectrometer in the wavenumber range 400 – 4000 cm^{-1} (the resolution of 1 cm^{-1}) with the KBr pellet technique. Tablets were prepared by mixing 1 mg of the studied material with 200 mg of KBr until obtaining a homogeneous mixture. Spectrophotometric analyses were carried out using UV/VIS LAMBDA 20 Perkin Elmer spectrophotometer.

2.5.7. Solid-state ^1H NMR

Solid-state ^1H NMR measurements of the spin-lattice relaxation times T_1 in the laboratory frame were performed on a pulse spectrometer operating at a frequency of 25 MHz (El-Lab Tel-Atomic) (Bilski et al., 2017). The measurement error was 3%. The samples of LOX, SBA-15-pr-NH_2:LOX and eSBA-15-pr-NH_2:LOX were sealed in the glass tubes and degassed to avoid humidity effects and to remove paramagnetic oxygen. The spin-lattice relaxation times T_1 were determined using the conventional saturation recovery sequence (Baranowski et al., 2011; Czechowski et al., 2012). Measurements were carried out in a wide temperature range from 80 K to 393 K. The temperature of the sample was controlled using a gas-flow cryostat and monitored with a Cernox resistor to an accuracy of 0.1 K. Due to a weak signal in SBA-15-pr-NH_2:LOX and eSBA-15-pr-NH_2:LOX samples related to a small number of protons, multiple-signal accumulation was applied.

2.6. Drug release studies

In vitro LOX release studies from adsorption systems and the dissolution tests of pure LOX were carried out on Electrolab EDT 08Lx apparatus at 37 ± 0.5 °C using a rotating paddle method (USP 2 apparatus). Due to the limited amount of material (samples weight corresponded to 4 mg of LOX), the volume of fluid was limited to 500 ml, while maintaining sink conditions. The mixing speed was set at 70 rpm. Four ml of dissolution fluid were removed from the vessel after 5, 15, 30, 60, 90 and 120 min and were immediately replaced by an appropriate volume of fresh medium at 37 ± 0.5 °C. The studies were performed in the following media: hydrochloric acidic medium at pH 1.2 ± 0.1, phosphate buffer at pH 6.8 ± 0.1 and phosphate buffer at pH 7.4 ± 0.1 (Ph. Eur. 10) The samples were filtered through 0.22 μm PTFE filters and LOX concentration was measured by UV spectrophotometry at 369 nm for pH 1.2 and 376 nm for phosphate buffers. All tests were performed in triplicate.

2.7. Cytotoxicity study

2.7.1. Cell culture

Caco-2 human colon adenocarcinoma cell line was purchased from the European Type Culture Collection (Sigma-Aldrich Co., St Louis, MO). The cells were maintained in phenol-free DMEM medium (Sigma-Aldrich Co., St Louis, MO), supplemented with 10/20% foetal bovine serum (FBS), 2 mM glutamine, penicillin (100 U/ml), streptomycin (0,1 mg/ml), and 1% non-essential amino acids mixture (Sigma-Aldrich Co., St Louis, MO). The experiments were performed with Caco-2 cells from the 20th to 29th passage.

2.7.2. Cell viability

Caco-2 cells were cultivated under the standard conditions at 37 °C in a humidified atmosphere containing 5% CO_2 and 95% air. To evaluate the effects of LOX, SBA-15-pr-NH_2 and SBA-15-pr-NH_2:LOX on cell viability, confluent stock cultures were detached using trypsin and seeded in 96-well plates at a density of 2×10^4 cells/well in 150 μl of growth medium. They were allowed to attach, and after 48 h the tested compounds were added. For the analysis we used the concentrations of SBA-15-pr-NH_2 in the range of 0.125 – 1.0 mg/ml and the LOX concentrations were equivalent to the amount of the compound adsorbed on SBA-15-pr-NH_2 used for the analysis. Cell viability was measured after 2 h of incubation using CellTiter-Glo® Luminescent Cell Viability Assay, according to the manufacturer's instruction.

3. Results and discussion

3.1. Drug incorporation

In this study we analysed the lornoxicam adsorption on two types of mesoporous silica: SBA-15 and SBA-15 modified with APTES using two various methods: adsorption equilibrium and solvent evaporation technique. We compared the process efficiency and the adsorption site of lornoxicam on the materials.

The texture of obtained materials before and after loading was analysed with the use of nitrogen adsorption–desorption analysis. The isotherms for SBA-15-pr-NH_2 with and without LOX loaded by both methods are shown in Fig. 1. Table 1 presents the structure parameters of the aforementioned samples and the unmodified SBA-15. According to the IUPAC classification, the obtained isotherms are consistent with the type IV isotherm characteristic of mesoporous adsorbents with microporous content. A H1 hysteresis loop confirms the presence of one dimensional cylindrical mesopores (Almáši et al., 2020; Esperanza Adrover et al., 2020; Moritz and Geszke-Moritz, 2015).

A pure SBA-15 sample demonstrated the highest specific surface area, pore volume and pore diameter. Reduction of all parameters after functionalization of the material is associated with the addition of aminopropyl groups on the surface. It is presumed that surface modification with aminopropyl groups occurs more easily in the area of the opening of mesopores and micropores, leading to their partial blockage and thus reduction of the surface area and pore volume (Goscianska et al., 2017). Surface functionalization also leads to a shift of capillary condensation towards lower pressures (Beňová et al., 2020). Likewise, the presence of adsorbed LOX molecules in the samples reduces all of the analysed values which is consistent with the literature (Eren et al., 2016).

The adsorption efficiency obtained by both methods is presented in Table 2. The results confirm the ability of analysed mesoporous

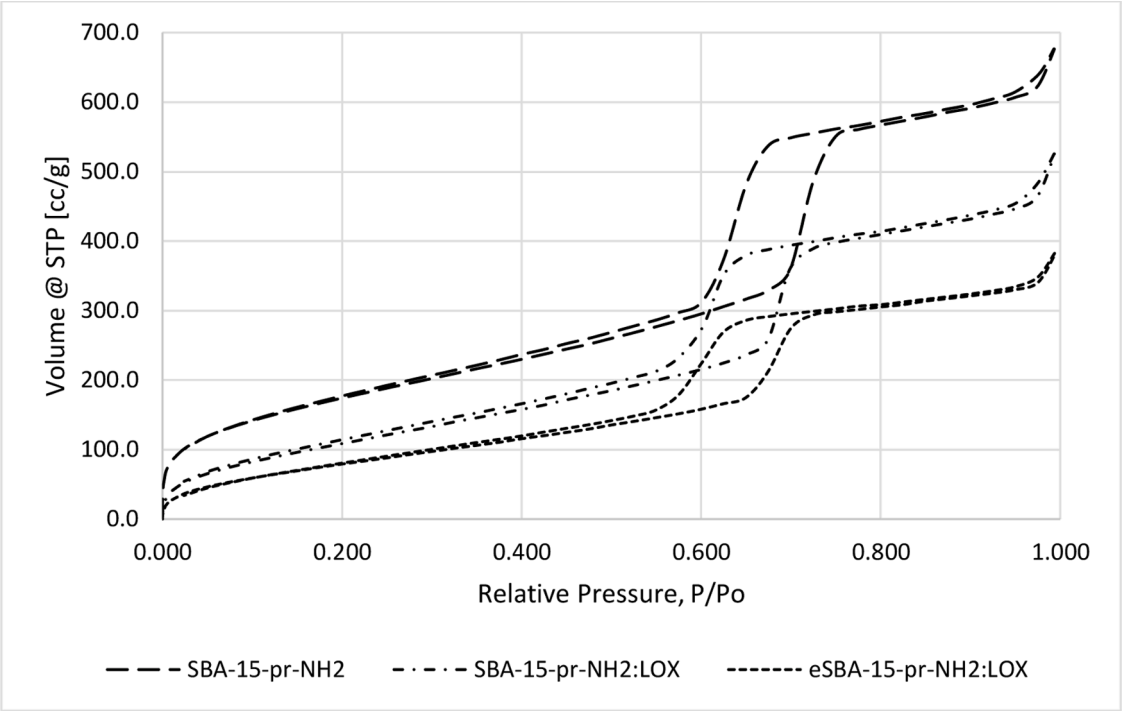

Fig. 1. N_2 adsorption/desorption isotherms of SBA-15-pr-NH_2, SBA-15-pr-NH_2:LOX and eSBA-15-pr-NH_2:LOX.

Table 1
Textural parameters of SBA-15, SBA-15-pr-NH_2, SBA-15-pr-NH_2:LOX and eSBA-15-pr-NH_2:LOX.

Sample	Specific surface area (SBET) [m^2/g]	Pore volume (Vp) [cm^3/g]	Pore diameter [nm]
SBA-15	798.00	1.010	6.0
SBA-15-pr-NH_2	644.34	0.997	5.8
SBA-15-pr-NH_2:LOX	447.54	0.820	5.4
eSBA-15-pr-NH_2:LOX	329.93	0.604	5.1

Table 2
The amount of adsorbed LOX into SBA-15 and SBA-15-pr-NH_2.

	SBA-15		SBA-15-pr-NH_2	
	UV [mg/g] ([%])	TGA [%]	UV [mg/g] ([%])	TGA [%]
adsorption equilibrium	–	–	42.39 (4.24)	4.20
solvent evaporation technique	224.65 (22.46)	22.62	266.49 (26.65)	26.85

materials to adsorb LOX. The amount of drug adsorbed on unmodified silica by adsorption equilibrium method is negligible and of no scientific value. The drug adsorption process is highly dependant on the interaction between the drug and the silica carrier. These interactions often involve electrostatic interactions and hydrogen bonds. The lack of LOX adsorption on SBA-15 silica, despite larger pore size, may be related to electrostatic interactions. SBA-15-pr-NH_2 has positively charged amino groups on its surface, while the surface of unmodified silica is negatively charged due to the presence of negatively charged silanol groups. The presence of a hydroxyl group in the LOX molecule corresponds to a negative surface charge, which ensures a much stronger binding to the positively charged surface of SBA-15-pr-NH_2 (Biswas, 2017; Eren et al., 2016).

In order to quantify the amount of LOX loaded on the silicas, we performed spectrophotometric analyses and applied the TGA method. The results are presented in Table 2. The amounts of adsorbed LOX obtained by spectrophotometric method are in agreement with the results of the TGA method.

Fig. 2 shows the TGA curves of LOX, SBA-15, SBA-15-pr-NH2, SBA-15-pr-NH2:LOX, eSBA-15:LOX and eSBA-15-pr-NH2:LOX. LOX was stable in the range between 35 and 150 °C. Above 200 °C a sharp decrease in the amount of LOX related to thermal single stage decomposition was observed causing 77.01% weight loss. The TGA curve for SBA-15 presented no change in the mass content. Pure SBA-15-pr-NH2 showed a total weight loss of 4.57% corresponding to the loss of organoamine groups. For the sample SBA-15-pr-NH2:LOX, we observed a mass loss of about 8.77% attributable to the loss of organoamine groups and the single stage decomposition of the adsorbed LOX. The TGA curves for the eSBA-15:LOX and eSBA-15-pr-NH2:LOX demonstrated the maximal single stage weight loss of 24.79% and 31.42%, respectively. This interpretation is consistent with previous publications (Abd-El-rahman et al., 2016; Ambrogi et al., 2007; Eren et al., 2016; Kiwilsza et al., 2013).

FT-IR spectroscopy identifies chemical bonds at molecule, determines the functional groups and confirms the presence of the adsorbate. This technique was used to investigate the interaction between the adsorbate and the silica matrix.

FT-IR spectra of LOX, APTES-modified mesoporous silica SBA-15 and its LOX loaded forms are shown in Fig. 3. Obtained results are consistent with the literature data (Thahir et al., 2019). In the spectrum of non-modified SBA-15, the broad band around 3430 cm^{-1} is associated with stretching vibrations of O—H groups (Si-OH). The band at 1638 cm^{-1} can be assigned to bending vibrations of O—H bonds in OH groups (Azimov et al., 2012) and also could be overlapped with C—O-C stretching vibrations. The asymmetric stretching vibrations of Si-O-Si are detected in the range 1100–1200 cm^{-1} and could be overlapped with Si-O-C, C—O-C and Si-C bond vibrations (Azimov et al., 2012). The band at 960 cm^{-1} corresponds to free silanol groups (Si-OH) on the surface of mesoporous silica (Goscianska et al., 2017). Symmetrical stretching vibrations of Si-O-Si bonds are identified at 800 cm^{-1} and its deformation vibrations at 465 cm^{-1} (Eren et al., 2016).

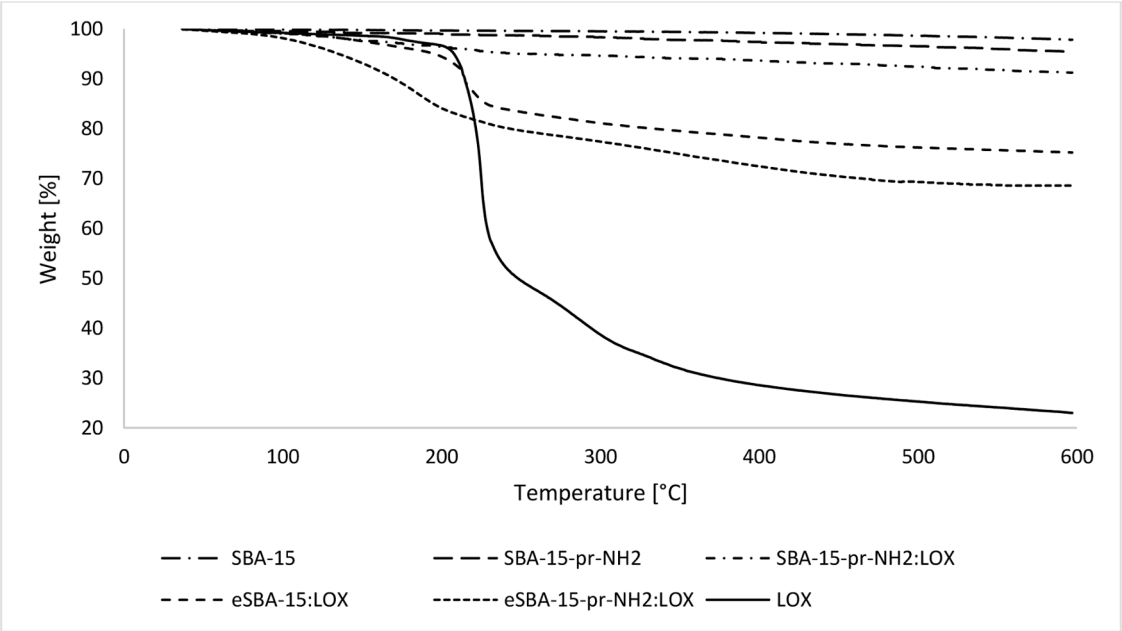

Fig. 2. TGA thermograms of SBA-15, SBA-15-pr-NH_2, SBA-15-pr-NH_2:LOX, eSBA-15:LOX, eSBA-15-pr-NH_2:LOX and LOX.

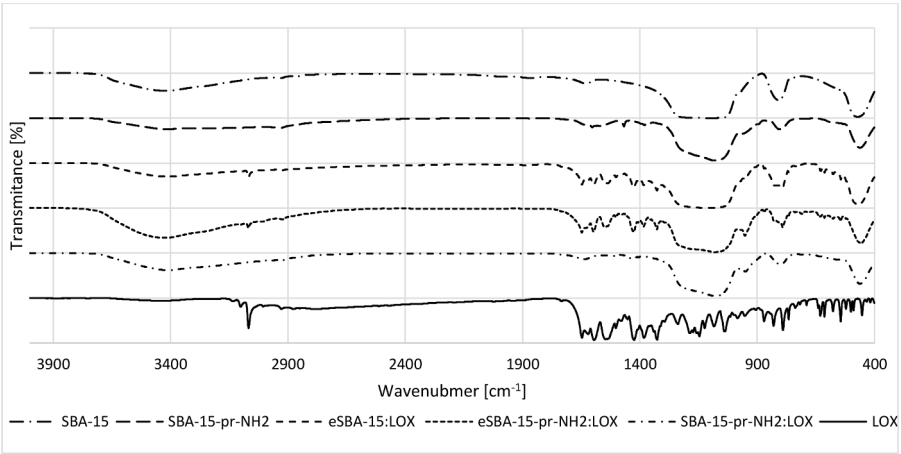

Fig. 3. FT-IR spectra of SBA-15, SBA-15-pr-NH_2, eSBA-15:LOX, eSBA-15-pr-NH_2:LOX, SBA-15-pr-NH_2:LOX and LOX.

The spectrum of the APTES-modified SBA-15 is similar. At 1500 cm^{-1} an additional band can be identified as bending vibrations of the N—H group. The stretching vibrations from the alkyl chain can be located at 2900 cm^{-1} (Szegedi et al., 2011) and the bending vibrations from CH_2 at 1405 cm^{-1}. In addition, the intensity of the stretching vibrations from the O—H group at 3600 cm^{-1} and bending vibrations at 1640 cm^{-1} are increased. Observed changes confirm the modification of the SBA-15 material (Goscianska et al., 2017).

In the spectrum of LOX, bands at 3064 cm^{-1} and 3102 cm^{-1} are assigned to C—H stretching vibrations of the aromatic ring. The peak at 1646 cm^{-1} corresponds to stretching vibrations of the carbonyl C = O group of the primary amide. The bending vibrations of the N—H bond in the secondary amide appear at 1596 cm^{-1} and 1621 cm^{-1}. The peaks identified at 1327 cm^{-1} and 1382 cm^{-1} are related to stretching vibrations of $O = S = O$. The C—N bonds can be detected at 1188 cm^{-1} and 1147 cm^{-1}. The band at 828 cm^{-1} is associated with stretching vibrations of C—Cl bond in the aliphatic chloro group of the LOX (Ahmed & Al-Badr, 2011).

The comparison FT-IR spectra of LOX, SBA-15 and SBA-15-pr-NH2 with SBA-15-pr-NH2:LOX and eSBA-15-pr-NH2:LOX spectra confirm the presence of the functional groups originating from LOX on the surface and inside mesoporous silica samples. For SBA-15-pr-NH2:LOX compared with silica new peaks at 1510 cm^{-1}, 1438 cm^{-1} and 710 cm^{-1} are detected, which means that the drug was adsorbed inside the pores of the silica. FT-IR spectrum for eSBA-15-pr-NH2:LOX reveals many more peaks characteristic of LOX, which suggests that when using the evaporation technique, the drug also covers the surface of silica.

Mesoporous materials contain mesopores, which can adsorb medicinal substances. Adsorption of the active substance in pores preserves an amorphous state, which improves its dissolution rate. Different techniques are investigated to obtain adsorption in pores. Our findings highlight that the employed adsorption method conditions the efficiency of the process. The obtained results indicate a higher efficiency of the solvent evaporation technique compared to the adsorption equilibrium method. However, during the adsorption via solvent evaporation the active substances can remain on the external surface of the silica without penetrating into its pores. This can result in a false increase in process efficiency. We conducted further investigation to assess whether LOX adsorption occurs on the silica surface or inside the mesopores.

The XRD analysis enables the identification of the crystalline and

amorphous state of drugs and carriers.

Small-angle XRD pattern of the modified SBA-15 is shown in Fig. 4A. The diffractogram presents three well-resolved peaks: one very intense diffraction peak at the value of 1° 2θ corresponding to (100) plane and two less intense reflections corresponding to (110) and (200) planes. The presence of these peaks confirms an ordered structure of hexagonal symmetry with the P6 mm space group. Our results are consistent with the data presented by Zhao et al. (Zhao et al., 1998).

The wide-angle diffractograms of all analysed samples are presented in Fig. 4B. The diffractogram of modified SBA-15 shows a wide peak (maximum at 22° 2θ) confirming the amorphous state of the analysed material (Kiwilsza et al., 2013). According to studies by Zhang et al., LOX exists in two polymorphic forms. The XRD patterns, as well as IR spectra, correspond to polymorph form II. The LOX diffractogram shows typical peaks located at 22.03°, 23.82°, 26.06°, 30.35° and 33.49° at the 2θ scale, which proves the crystalline form of pure LOX. The absence of the aforementioned peaks on diffractogram of SBA-15-pr-NH_2:LOX confirms the amorphous state of LOX after loading with adsorption equilibrium method (Almáši et al., 2020; Zhang et al., 2013). Moreover, it proves that the adsorption took place inside the silica mesopores (Guo et al., 2013; Pardhi et al., 2017). The diffraction patterns of the samples obtained by the solvent evaporation method show a broad band assigned to the silica carrier and the characteristic peaks of LOX, although their intensity is lower than for the pure compound. The peaks corresponding to the crystalline LOX are more intense in the eSBA-15:LOX sample compared to the eSBA-15-pr-NH_2:LOX. This may indicate that the drug after adsorption on SBA-15-pr-NH_2 was partially adsorbed inside the mesopores, whereas on the SBA-15, the adsorption occurred only on the surface of the material. The obtained results indicate that the solvent evaporation method does not ensure optimal drug adsorption and its stabilization in the amorphous form.

Similar conclusions were provided by the DSC method. DSC allows the evaluation of the physical state of the samples and describes their thermal properties. It is used to determine glass transitions and to investigate the melting and crystallization behaviour of materials. The DSC curves for LOX, SBA-15, SBA-15-pr-NH_2, SBA-15-pr-NH_2:LOX, eSBA-15:LOX and for eSBA-15-pr-NH_2:LOX are presented in Fig. 5. For pure LOX, no endothermic melting peak was found but according to the literature data (Nijhawan et al., 2014; Zhang et al., 2013) melting and decomposition processes occurring simultaneously as well as the

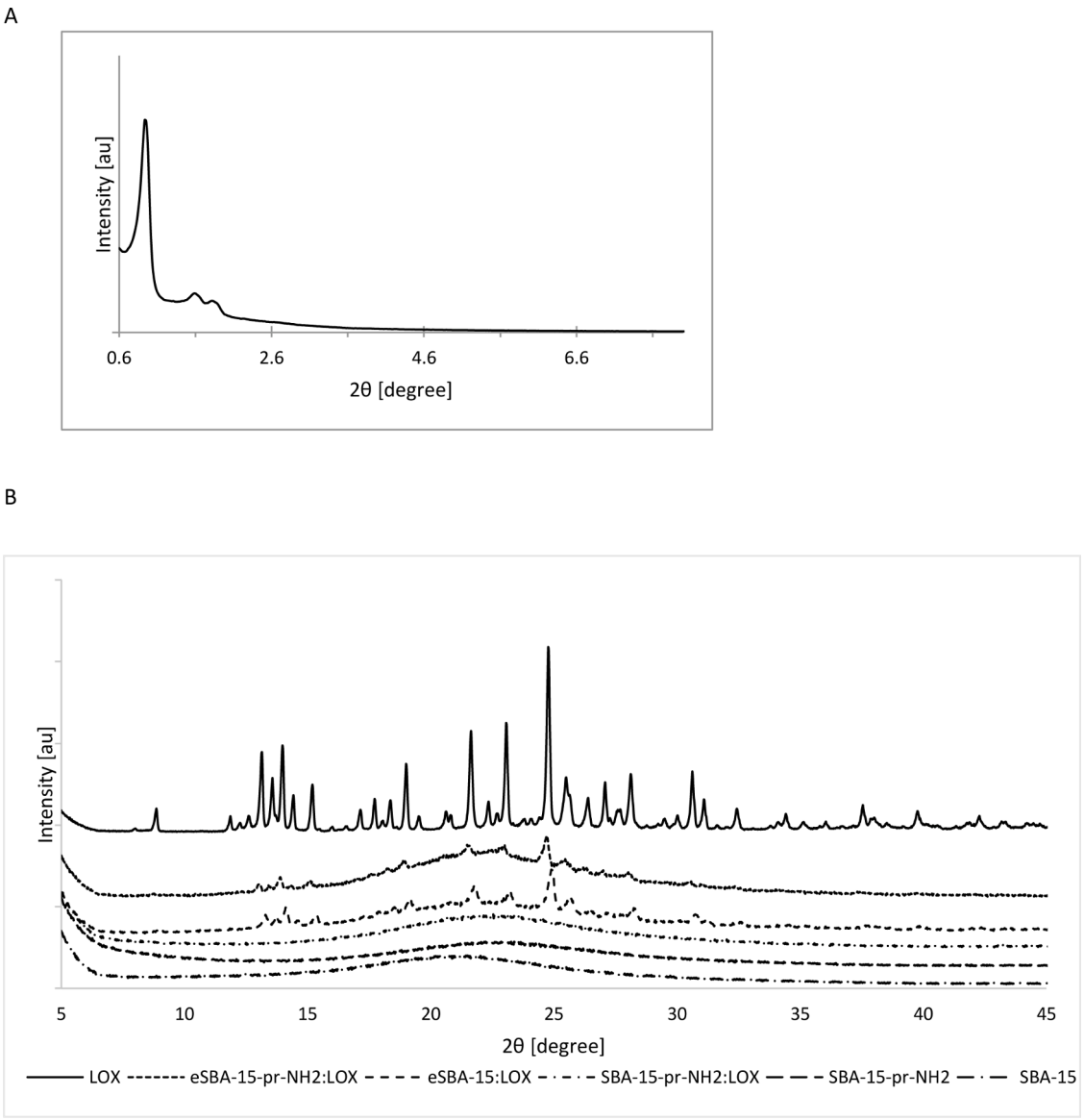

Fig. 4. (A) Small-angle X-ray diffraction pattern of the SBA-15-pr-NH_2, (B) Wide-angle XRD diffractograms of LOX, eSBA-15-pr-NH_2:LOX, eSBA-15:LOX, SBA-15-pr-NH_2:LOX, SBA-15-pr-NH_2, and SBA-15.

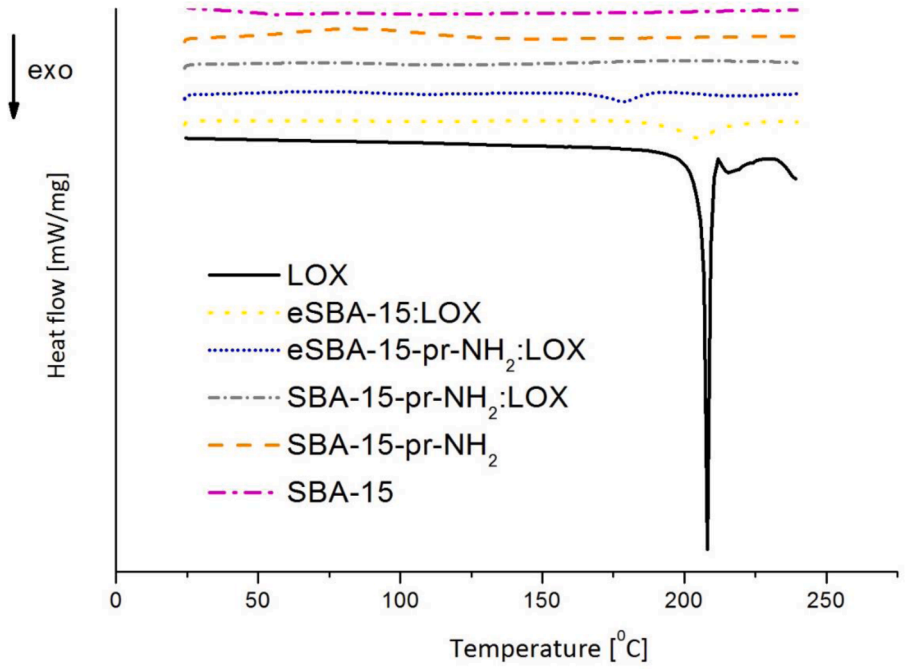

Fig. 5. DSC thermograms of SBA-15, SBA-15-pr-NH_2, SBA-15-pr-NH_2:LOX, eSBA-15:LOX, eSBA-15-pr-NH_2:LOX and LOX.

thermogram for LOX exhibit a sharp exothermic peak around 210 °C, which confirms the crystalline nature of the sample.

The DSC curves for mesoporous silica samples showed a peak associated with glass transition at 348 K (75 °C) for SBA-15 and at 338 K (65 °C) for SBA-15-pr-NH_2, which proves their amorphous state. In the investigated temperature range we observed no melting peak of samples which goes to prove thermal stability up to a temperature of 523 K (250 °C) (Thahir et al., 2019).

The decrease in the glass transition temperature Tg could be attributed to the weakening of intramolecular interactions in the modified silica, which is supported by the results of FT-IR study.

Similarly, the sample with incorporated LOX by adsorption equilibrium method showed no melting and decomposition peaks, which confirms that LOX is adsorbed inside the pores of SBA-15-pr-NH_2 in an amorphous state (Pardhi et al., 2017; Wang et al., 2014).

For samples obtained by evaporation method (eSBA-15-pr-NH_2:LOX,

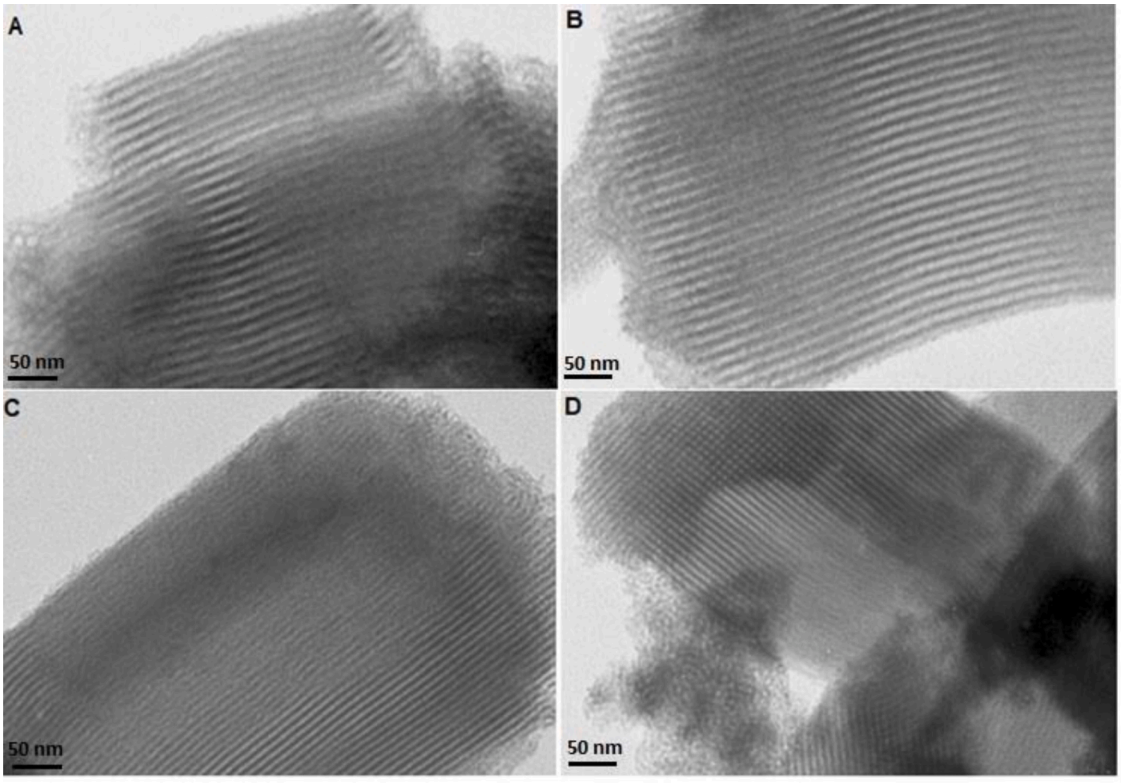

Fig. 6. TEM images of A. SBA-15, B. SBA-15-pr-NH_2, C. SBA-15-pr-NH_2:LOX, D. eSBA-15-pr-NH_2:LOX.

eSBA-15:LOX), in DSC curves apart from the peak associated with Tg, two exothermic peaks corresponding to the decomposition of LOX were observed (179 °C and 206 °C, respectively) but no melting point was shown. We assume that the first decomposition peak, shifted to lower temperatures compared to pure LOX, covered the melting peak, which is consistent with the literature data (Thahir et al., 2019). The shift towards lower temperatures of both the Tg and the peaks associated with decomposition is evidence of a reduction in intermolecular interactions in the pure LOX. Moreover, the shift is due to the fact that LOX is partially in an amorphous state and the LOX on the external surface of silica formed crystals of a smaller size due to space limitations (Eren et al., 2016; Guo et al., 2013; Pardhi et al., 2017). These results are in agreement with the results of XRD analysis.

Subsequent methods allowed us to evaluate the texture and morphology of the samples. The structure of the obtained materials was determined using transmission electron microscopy (TEM). TEM images of silica samples with and without LOX (except eSBA-15:LOX) are presented in Fig. 6 TEM imaging showed the presence of parallel mesoporous channels, which confirms the two-dimensional structure of the material (Esperanza Adrover et al., 2020; Meynen et al., 2009). The APTES functionalization did not influence the initial structure of SBA-15. Moreover, the structure of silica carriers did not change after LOX application. Our results are consistent with the literature data (Almáši et al., 2020; Eren et al., 2016; Esperanza Adrover et al., 2020; Moritz and Geszke-Moritz, 2015).

The SEM (scanning electron microscopy) analysis allowed to assess the morphology of the tested materials' particles. The SEM micrographs A-C and E (Fig. 7) show well-formed, oval, rod-like shape particles with a size of about 1 μm. Individual grains combine to form larger structures resembling linear chain. Obtained micrographs are consistent with the literature data (Eren et al., 2016; Esperanza Adrover et al., 2020). The SEM micrograph of eSBA-15:LOX shows crystals larger than single grains of SBA-15 silica. These are crystals of unadsorbed LOX formed during the evaporation of the solvent, which indicates a failure of LOX adsorption into the silica pores. The solvent evaporation method is not an effective method of adsorbing LOX into the pores of unmodified SBA-15 silica as confirmed in the XRD and DSC analysis.

Finally, the solid-state ^{1}H NMR spectroscopy was employed to confirm the change of the crystalline structure of the drug incorporated into the mesoporous silica, which was revealed by changing the molecular dynamics. The temperature dependence of the spin-lattice relaxation times T_1 in the laboratory frame provides information on

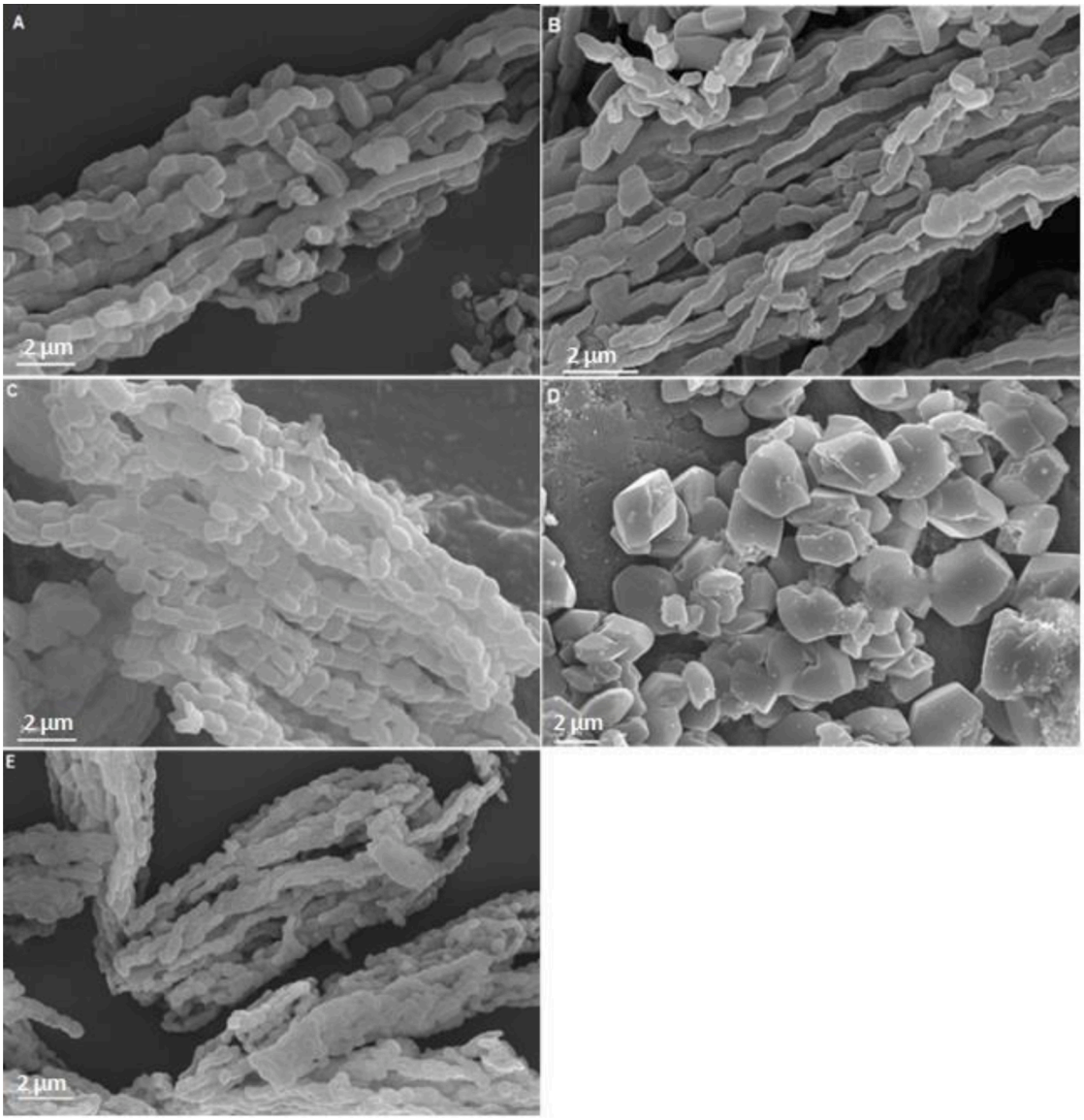

Fig. 7. SEM images of A. SBA-15, B. SBA-15-pr-NH_2, C. SBA-15-pr-NH_2:LOX, D. eSBA-15:LOX, E. eSBA-15-pr-NH_2:LOX.

variations of the relaxation processes and structure of the investigated samples (Makrocka-Rydzyk et al., 2015; Woźniak-Braszak et al., 2019).

For LOX and for SBA-15-pr-NH_2:LOX the recovery of magnetization $M_z(t)$ was one-exponential in the entire temperature range. The spin-relaxation time T_1 was estimated from fitting the following equation to the experimental data:

$$\frac{M_0 - M_z(t)}{M_0} = exp\left(-\frac{t}{T_1}\right), \quad (1)$$

where: M_o is the equilibrium magnetization, T_1 is the relaxation time.

For eSBA-15-pr-NH_2:LOX sample, the recovery of the magnetization was bi-exponential resulting in two magnetization fractions that needed to be described by the formula:

$$\frac{M_0 - M_z(t)}{M_0} = M01exp\left(-\frac{t}{T_{1L}}\right) + M02exp\left(-\frac{t}{T_{1S}}\right), \quad (2)$$

where: M_o is the equilibrium magnetization, T_{1L} is the long and T_{1S} is short relaxation time, and *M01* and *M02* are magnetization fractions of long and short component, respectively.

The bi-exponential recovery of the magnetization indicates an occurrence of two isolated spin systems with different relaxation times. The long T_{1L} and short T_{1S} components of relaxation times are connected with the existence of different phases with various structures and molecular dynamics. Moreover, the values of M01 and M02 magnetization fractions are proportional to the number of protons contained in individual systems (Dobrzyńska-Mizera et al., 2020; Kiwilsza et al., 2017).

The temperature dependences of proton spin-lattice relaxation times T_1 in the laboratory frame obtained at frequencies 25 MHz for the LOX, SBA-15-pr-NH_2:LOX and eSBA-15-pr-NH_2:LOX samples are depicted in Fig. 8. For LOX, one broad and an asymmetrical minimum of 70 ms at about 115 K (−158 °C) is presented. According to previous NMR studies (Dobrzyńska-Mizera et al., 2020; Holderna-Natkaniec et al., 2005; Woźniak-Braszak et al., 2019) this minimum at a low temperature could be associated with the rotation of methyl (CH_3) groups around its threefold axes C3. Because, in the high-temperature region, a change in the slope of T_1 versus 10^3/T is observed, the contribution of another type of molecular motion has been taken into account.

For SBA-15-pr-NH_2:LOX the relaxation times are shorter compared to pure LOX and also show a broad and asymmetrical minimum of 64 ms, but at the higher temperature of 140 K (−132 °C). Having regard to changes in the slope of relaxation times both at high and low temperatures, apart from the motion of the CH_3 groups, two additional molecular motions were taken into account for the interpretation of the relaxation processes of the LOX incorporated into the silica by the adsorption method. It is assumed that in the low temperature range, molecular dynamics include jumps of hydrogen atoms in hydrogen bonds (Holderna-Natkaniec et al., 2006).

NMR data for eSBA-15-pr-NH_2:LOX revealed bi-exponential magnetization recovery which proves the existence of two separately relaxing phases of the drug. The ratio of the magnetization fractions associated with T_{1L} and T_{1S} was 3/7 throughout the tested temperature range. These two relaxation times possess similar reciprocal temperature dependence. For the long component T_{1L}, the broad and asymmetrical minimum appears in a similar temperature range and has a similar value to the minimum relaxation times for Lox. In the case of the short component of relaxation times T_{1S}, gradually decrease reaching a wide minimum of around 90 K (−182 °C). It is assumed that the long relaxation time T_{1L} is related to the drug located outside the pores, while the T_{1S} fraction is associated with confided LOX inside the pores.

Based on the experimental data it was determined that 30% of the drug is localized outside the pores and about 70% inside. Obtained results are consistent with our DSC and XRD analyses which confirmed partial adsorption on the silica's surface.

The activation parameters describing molecular dynamics of LOX, SBA-15-pr-NH_2:LOX and eSBA-15-pr-NH_2:LOX samples were determined by analysing the temperature dependence of spin-relaxation times T_1 in terms of the dipol-dipol Bloembergen–Purcell–Pound (BPP) theory (Bloembergen et al., 1948). It was assumed that the T_1 values were determined by dipolar interactions modulated by different molecular processes. Taking into account all contributions, T_1 was determined using Eq. (3) (Abragam, 1961; Slichter, 1990):

$$\frac{1}{T_1} = \frac{2}{3}\gamma^2 \sum_k \Delta M_{2k}[J_k(\omega) + 4J_k(2\omega)] \quad (3)$$

where: γ is a gyromagnetic ratio of protons, ΔM_{2k} is a part of the second moment averaged by motions under consideration, and $J_k(\omega)$ denotes

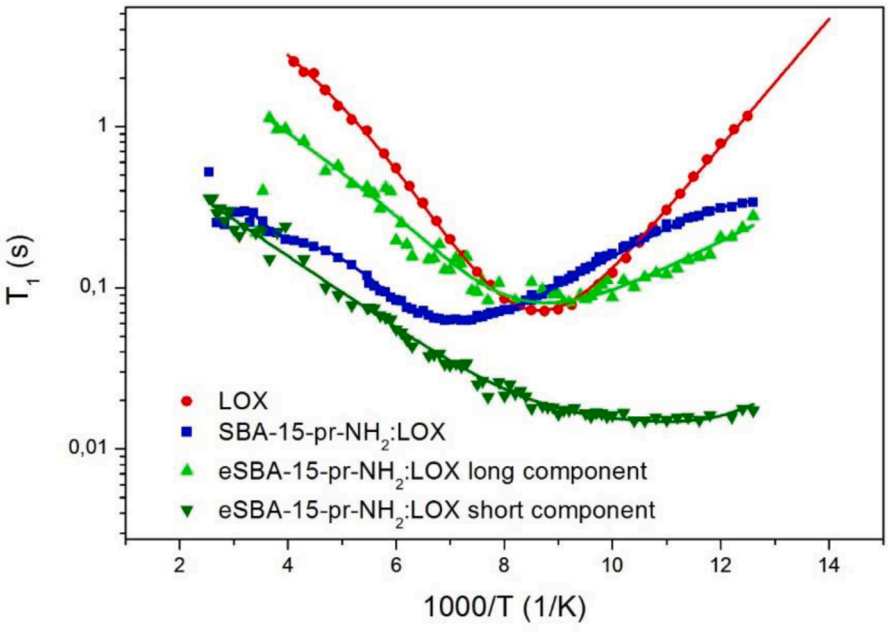

Fig. 8. Temperature dependence of the spin-relaxation time T1 in the laboratory frame for LOX, SBA-15-pr-NH_2:LOX and eSBA-15-pr-NH_2:LOX (long and short components). The solid lines are the best fits of Eq. (2) to the data.

the spectral density function for the angular frequency ω.

To describe a broad and asymmetrical minimum of relaxation times T_1 associated with the motion of the CH_3 groups the spectral density function J(ω), given by Davidson and Cole, was used (Davidson and Cole, 1951):

$$J(\omega,\tau_c,\beta)=\frac{2}{\omega}\left[\frac{sin(\beta arctan(\omega\tau_c))}{\left(1+\omega^2\tau_c^2\right)^{\frac{\beta}{2}}}\right], \quad (4)$$

where: τ_c is the upper cut-off correlation time and β is the distribution width of correlation times.

Taking into account that motions are thermally activated, the temperature dependence of the correlation time τ_c could be expressed by the Arrhenius formula:

$$\tau_c=\tau_0 exp\left(\frac{E_a}{RT}\right), \quad (5)$$

where: τ_0 is the pre-exponential factor, E_a is the activation energy of molecular motion, and R is the universal gas constant.

To the interpretation of the additional local motions at high and low temperatures the classical BPP spectral density function was applied (Beckmann, 1988):

$$J(\omega)=\frac{2\tau_c}{1+\omega^2\tau_c^2}. \quad (6)$$

By fitting the Eq. (3-6) to the experimental points depicted in Fig. 8, the activation parameters of the assumed molecular motions were determined. The solid lines in Fig. 8 show the result of the best numerical fit. The activations parameters are summarized in Table 3.

Different temperature T1 curves for SBA-15-pr-NH_2:LOX and eSBA-15-pr-NH_2:LOX in comparison to LOX indicate a change in the molecular structure and dynamics of drug encapsulated in mesoporous silica. Considering activation parameters it can be concluded that assuming relaxation processes for incorporated LOX appear at the higher temperature, which means molecular dynamics is hindered for molecules of LOX inside the pores. The NMR results show that the activation energies of the rotation of the CH_3 groups and local motions decrease for the drug introduced into the silica pores. What is more the reduction of the second moment is greater for the incorporated drug, which indicates the increased mobility of these systems and confirms the change of the structure from crystalline to amorphous (Pajzderska i in., 2019), which is in agreement with the results of the DSC and XRD analysis.

Table 3
Motional parameters obtained for LOX, SBA-15-pr-NH_2:LOX and eSBA-15-pr-NH_2:LOX (long and short components). The solid lines are the best fits of Eq. (3-6) to the experimental data. The values of the uncertainty of the estimated parameters were lower than 10%. T_{1L} is the long and T_{1S} is the short relaxation time, τ_0 is the pre-exponential factor, E_a is the activation energy of molecular motions, and β is the distribution width of correlation times.

Sample	Rotation of Methyl Groups CH_3 Around Their Axes Symmetries	Motion in high temperature	Motion in low temperature
LOX	$\tau_{01}=3.8\times10^{-13}$ [s] $E_{a1}=8.9$ [kJ/mol] $\Delta M_1=3.5$ [Gs^2] $\beta=0.9$	$\tau_{02}=4.2\times10^{-10}$ [s] $E_{a2}=5.1$ [kJ/mol] $\Delta M_2=0.1$ [Gs^2]	
SBA-15-pr-NH_2:LOX	$\tau_{01}=7.9\times10^{-12}$ [s] $E_{a1}=7.9$ [kJ/mol] $\Delta M_1=5.0$ [Gs^2] $\beta=0.5$	$\tau_{02}=5.2\times10^{-11}$ [s] $E_{a2}=4.8$ [kJ/mol] $\Delta M_2=0.4$ [Gs^2]	$\tau_{03}=4.5\times10^{-14}$ [s] $E_{a3}=5.2$ [kJ/mol] $\Delta M_3=4.1$ [Gs^2]
eSBA-15-pr-NH_2:LOX long component T_{1L}	$\tau_{01}=3.9\times10^{-12}$ [s] $E_{a1}=7.1$ [kJ/mol] $\Delta M_1=4.0$ [Gs^2] $\beta=0.5$	$\tau_{02}=5.4\times10^{-10}$ [s] $E_{a2}=3.7$ [kJ/mol] $\Delta M_2=0.1$ [Gs^2]	
eSBA-15-pr-NH_2:LOX short component T_{1S}	$\tau_{01}=3.8\times10^{-13}$ [s] $E_{a1}=6.8$ [kJ/mol] $\Delta M_1=15$ [Gs^2] $\beta=0.7$	$\tau_{02}=3.2\times10^{-11}$ [s] $E_{a2}=4.3$ [kJ/mol] $\Delta M_2=2.8$ [Gs^2]	

3.2. Drug release studies

Fig. 9 shows LOX release profiles from mesoporous materials at different pH compared to dissolution of the crystalline form of LOX. The LOX release from the analysed materials was studied in phosphate buffers at pH 7.4 and 6.8 and in hydrochloric acidic medium at pH 1.2 because the drug release depends on the pH (Gadade et al., 2017). As the pH increases, the solubility of LOX increases and the differences between release profiles from silica and crystalline LOX diminish. At all pH values during a 30 min period, more LOX was released from silicas compared to the amount of dissolved crystalline form. It may be related to the properties of SBA-15-pr-NH_2 ensuring that the adsorbed drug remains in a more soluble amorphous form (Biswas, 2017). Subsequent time intervals favour the dissolution of crystalline LOX at a higher pH. All release profiles of LOX from silicas are characterized by the initial burst release, followed by prolonged release rate. The initial burst may be associated with the presence of LOX molecules inside the mesopores that were weakly bound. By contrast, the extended release of the remaining LOX is due to the presence of stronger interactions between LOX molecules and aminopropyl groups (Song et al., 2005).

The differences in the release profiles were most evident in hydrochloric acidic medium at pH 1.2. In this medium, the drug release from modified silica of 30% was achieved after 5 min, while the dissolution of crystalline LOX did not reach this level even after 120 min of the test (less than 19%). Such significant differences in the release profiles are related to the change in LOX solubility and to the pH of the environment. The more acidic pH, the lower solubility of the LOX was observed (Gadade et al., 2017). Consequently, the beneficial influence of LOX adsorption on SBA-15-pr-NH_2 on the drug dissolution rate was more apparent at lower pHs where LOX solubility is decreased. For buffer of pH 7.4, no differences in release profiles were obtained between the silica and the dissolution of the crystalline form. The value of the coefficient f2 was 32.45 for hydrochloric acidic medium at pH 1.2 and for phosphate buffers 42.21 and 57.25 for pH 6.8 and pH 7.4, respectively.

3.3. Cytotoxicity study

The biocompatibility of orally administered drugs can be assessed using cell viability tests. For this study, we used human colorectal adenocarcinoma cells Caco-2, which are morphologically and physiologically comparable to the intestinal epithelial cells (Letchmanan et al., 2015). Fig. 10 demonstrates the viability of Caco-2 cells after 2 h exposure to SBA-15-pr-NH_2, SBA-15-pr-NH_2:LOX (0.125, 0.25, 0.50, 1.0 mg/ml) and LOX (0.0053, 0.0106, 0.0212, 0.0424 mg/ml). None of the analysed samples manifested harmful effects on the cells in the tested concentrations. We observed no significant differences between the cell viability of each sample, which allows us to conclude that adsorption of LOX to SBA-15 did not alter the cytotoxicity of the silica itself. Presented results are in line with previous reports by Heikkilä et al. (Heikkilä et al., 2010).

4. Conclusion

In our study, we successfully obtained SBA-15 silica and functionalised its surface with 3-aminopropyl groups. Further research plans are to analyse the influence of other silica's surface modifications on the adsorption efficiency. The introduction of other functional groups may lead to an increase in the interactions between the drug and silica, resulting in greater amount of adsorbed drug. In presented study we

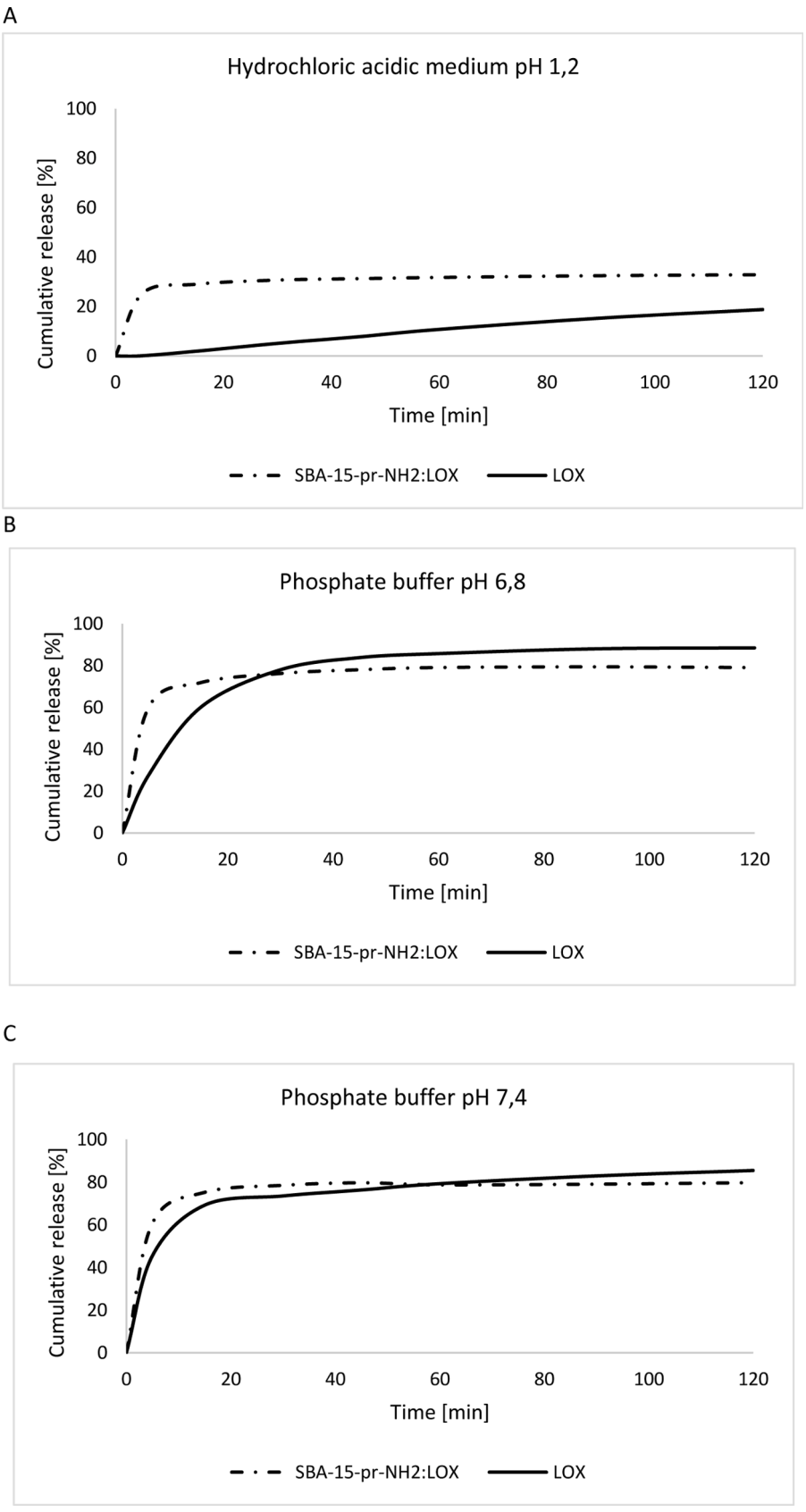

Fig. 9. Dissolution profile of LOX and SBA-15-pr-NH_2:LOX.

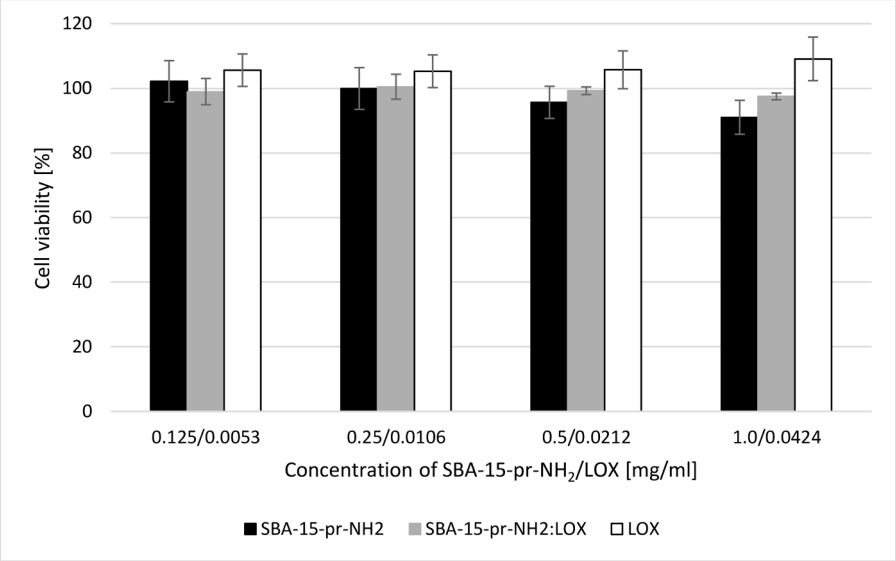

Fig. 10. Caco-2 cell viability results after 2 h incubation with SBA-15-pr-NH_2, SBA-15-pr-NH_2:LOX and LOX at 37 °C.

investigated two methods of LOX adsorption on both of the obtained materials. Although the solvent evaporation method resulted in a higher amount of adsorbed LOX, it is not suitable due to the adsorption of the drug on the outer surface of the material in crystalline state in 30%. We proved that the adsorption equilibrium is a favourable method, which ensures the adsorption of LOX inside the mesopores. In our study, we analysed two of the most commonly used drug loading methods. Future research may include further analysis of available literature methods in order to find the most desirable one. Here, we confirmed the desirable adsorption by SEM, DSC, XRD and ^{1}H NMR analysis. LOX adsorbed on SBA-15-pr-NH_2 demonstrated a higher dissolution rate at acidic pH compared to pure LOX. Further studies are required to evaluate the stability of the obtained systems and the amorphous form of the adsorbed LOX. The cytotoxicity of modified SBA-15 both with and without adsorbed lornoxicam is negligible. Our study proves that SBA-15 is applicable as an effective and non-toxic carrier for the poorly soluble drug lornoxicam.

CRediT authorship contribution statement

Adrianna Dadej: Methodology, Validation, Formal analysis, Investigation, Writing – original draft, Writing – review & editing, Visualization. **Aneta Woźniak-Braszak:** Investigation. **Paweł Bilski:** Investigation. **Hanna Piotrowska-Kempisty:** Methodology, Investigation. **Małgorzata Józkowiak:** Investigation. **Anna Pawełczyk:** Investigation. **Daniela Dadej:** Writing – review & editing. **Dominika Łażewska:** Investigation. **Anna Jelińska:** Conceptualization, Methodology, Writing – review & editing, Supervision.

Declaration of Competing Interest

The authors declare that they have no conflict of interest.

Acknowledgements

We thank Dr. M. Geszke-Moritz and Dr. M. Moritz from Pomeranian Medical University in Szczecin for the synthesis and functionalization of SBA-15.

Funding

This research did not receive any specific grant from funding agencies in the public, commercial, or not-for-profit sectors.

References

Abd-Elrahman, A.A., El Nabarawi, M.A., Hassan, D.H., Taha, A.A., 2016. Ketoprofen mesoporous silica nanoparticles SBA-15 hard gelatin capsules: preparation and in vitro/in vivo characterization. Drug Deliv. 23 (9), 3387–3398. https://doi.org/10.1080/10717544.2016.1186251.

Abragam, A., 1961. The Principles of Nuclear Magnetism. Clarendon Press.

Almáši, M., Beňová, E., Zeleňák, V., Madaj, B., Huntošová, V., Brus, J., Urbanová, M., Bednarčík, J., Hornebecq, V., 2020. Cytotoxicity study and influence of SBA-15 surface polarity and pH on adsorption and release properties of anticancer agent pemetrexed. Mater. Sci. Eng.: C 109, 110552. https://doi.org/10.1016/j.msec.2019.110552.

Anu Prathap, M.U., Kaur, B., Srivastava, R, 2012. Direct synthesis of metal oxide incorporated mesoporous SBA-15, and their applications in non-enzymatic sensing of glucose. J. Colloid Interface Sci. 381 (1), 143–151. https://doi.org/10.1016/j.jcis.2012.05.025.

Baranowski, M., Woźniak-Braszak, A., Jurga, K., 2011. High homogeneity B(1) 30.2MHz Nuclear Magnetic Resonance Probe for off-resonance relaxation times measurements. J. Magn. Reson. (San Diego, Calif. 208 (1), 163–166. https://doi.org/10.1016/j.jmr.2010.10.018, 1997).

Beckmann, P.A., 1988. Spectral densities and nuclear spin relaxation in solids. Phys. Rep. 171 (3), 85–128. https://doi.org/10.1016/0370-1573(88)90073-7.

Beňová, E., Bergé-Lefranc, D., Zeleňák, V., Almáši, M., Huntošová, V., Hornebecq, V., 2020. Adsorption properties, the pH-sensitive release of 5-fluorouracil and cytotoxicity studies of mesoporous silica drug delivery matrix. Appl. Surf. Sci. 504, 144028 https://doi.org/10.1016/j.apsusc.2019.144028.

Bilski, P., Drużbicki, K., Jenczyk, J., Mielcarek, J., Wasicki, J., 2017. Molecular and Vibrational Dynamics in a Cholesterol-Lowering Agent Lovastatin: solid-State NMR, Inelastic Neutron Scattering and Periodic DFT Study. J. Phys. Chem. B 121. https://doi.org/10.1021/acs.jpcb.7b01090.

Biswas, N., 2017. Modified mesoporous silica nanoparticles for enhancing oral bioavailability and antihypertensive activity of poorly water soluble valsartan. Eur. J. Pharm. Sci. 99, 152–160. https://doi.org/10.1016/j.ejps.2016.12.015.

Bloembergen, N., Purcell, E.M., Pound, R.V., 1948. Relaxation effects in nuclear magnetic resonance absorption. Phys. Rev. 73 (7), 679–712. https://doi.org/10.1103/PhysRev.73.679.

Brus, J., Albrecht, W., Lehmann, F., Geier, J., Czernek, J., Urbanova, M., Kobera, L., Jegorov, A., 2017. Exploring the molecular-level architecture of the active compounds in liquisolid drug delivery systems based on mesoporous silica particles: old tricks for new challenges. Mol. Pharm. 14 (6), 2070–2078. https://doi.org/10.1021/acs.molpharmaceut.7b00167.

Byrav, P., Medhi, B., Prakash, Patyar, S., Wadhwa, S, 2009. Lornoxicam: a newer NSAID. Indian J. Phys. Med. Rehab. 20.

Chaudhary, V., Sharma, S., 2017. An overview of ordered mesoporous material SBA-15: synthesis, functionalization and application in oxidation reactions. J. Porous Mater. 24 (3), 741–749. https://doi.org/10.1007/s10934-016-0311-z.

Czechowski, T., Baranowski, M., Woźniak-Braszak, A., Jurga, K., Jurga, J., Kędzia, P., 2012. The instrument set for generating fast adiabatic passage. Appl. Magn. Reson. 43 (3), 331–340. https://doi.org/10.1007/s00723-012-0372-3.

Davidson, D.W., Cole, R.H., 1951. Dielectric relaxation in glycerol, propylene glycol, and n-propanol. J. Chem. Phys. 19 (12), 1484–1490. https://doi.org/10.1063/1.1748105.

Dobrzyńska-Mizera, M., Knitter, M., Woźniak-Braszak, A., Baranowski, M., Sterzyński, T., Di Lorenzo, M.L., 2020. Poly(l-lactic acid)/pine wood bio-based composites. Materials (Basel) 13 (17), 3776. https://doi.org/10.3390/ma13173776.

Eren, Z.S., Tunçer, S., Gezer, G., Yildirim, L.T., Banerjee, S., Yilmaz, A., 2016. Improved solubility of celecoxib by inclusion in SBA-15 mesoporous silica: drug loading in different solvents and release. Microporous Mesoporous Mater. 235, 211–223. https://doi.org/10.1016/j.micromeso.2016.08.014.

Esperanza Adrover, M., Pedernera, M., Bonne, M., Lebeau, B., Bucalá, V., Gallo, L, 2020. Synthesis and characterization of mesoporous SBA-15 and SBA-16 as carriers to improve albendazole dissolution rate. Saudi Pharmaceut. J.: SPJ: Off. Publ. Saudi Pharmaceut. Soc. 28 (1), 15–24. https://doi.org/10.1016/j.jsps.2019.11.002.

Gadade, D.D., Kulkarni, D.A., Rathi, P.B., Pekamwar, S.S., Joshi, S.S., 2017. Solubility Enhancement of Lornoxicam by Crystal Engineering. Indian J. Pharm. Sci. 79 (2), 277–286. https://doi.org/10.4172/pharmaceutical-sciences.1000226.

Goscianska, J., Olejnik, A., Nowak, I., 2017. APTES-functionalized mesoporous silica as a vehicle for antipyrine – adsorption and release studies. Colloids Surf. A 533, 187–196. https://doi.org/10.1016/j.colsurfa.2017.07.043.

Guo, Z., Liu, X.-.M., Ma, L., Li, J., Zhang, H., Gao, Y.-.P., Yuan, Y., 2013. Effects of particle morphology, pore size and surface coating of mesoporous silica on Naproxen dissolution rate enhancement. Colloids Surf. B Biointerfaces 101, 228–235. https://doi.org/10.1016/j.colsurfb.2012.06.026.

Hamza, Y.E.-S., Aburahma, M.H., 2009. Design and in vitro evaluation of novel sustained-release double-layer tablets of lornoxicam: utility of cyclodextrin and xanthan gum combination. AAPS PharmSciTech. 10 (4), 1357–1367. https://doi.org/10.1208/s12249-009-9336-9.

Heikkilä, T., Santos, H.A., Kumar, N., Murzin, D.Y., Salonen, J., Laaksonen, T., Peltonen, L., Hirvonen, J., Lehto, V.-.P., 2010. Cytotoxicity study of ordered mesoporous silica MCM-41 and SBA-15 microparticles on Caco-2 cells. Eur. J. Pharmaceut. Biopharmaceut.: Off. J. Arbeitsgemeinschaft Fur Pharmazeutische Verfahrenstechnik e.V 74 (3), 483–494. https://doi.org/10.1016/j.ejpb.2009.12.006.

Holderna-Natkaniec, K., Jurga, K., Natkaniec, I., Nowak, D., Szyczewski, A., 2005. Molecular dynamics of ethisterone studied by 1H NMR, IINS and quantum mechanical calculations. Chem. Phys. 317, 178–187. https://doi.org/10.1016/j.chemphys.2005.06.043.

Holderna-Natkaniec, K., Natkaniec, I., Kasperkowiak, W., Sciesinska, E., Sciesinski, J., Mikuli, E., 2006. The IINS, IR and DFT studies of hydrogen bonds in 6-Furfuryl and 6-Benzylaminopurines. J. Mol. Struct. 790 (1), 94–113. https://doi.org/10.1016/j.molstruc.2005.11.042.

Kim, S.-.N., Ko, S.A., Lee, S.H., Huh, B.K., Choy, Y.B., 2018. Amine-grafted SBA-15 for ophthalmic delivery of dexamethasone. J. Solid State Chem. 268, 102–107. https://doi.org/10.1016/j.jssc.2018.08.036.

Kiwilsza, A., Mielcarek, J., Pajzderska, A., Wąsicki, J., 2013. Ordered mesoporous silica material SBA-15: loading of new calcium channel blocker–lacidipine. J. Microencapsul. 30 (1), 21–27. https://doi.org/10.3109/02652048.2012.692401.

Kiwilsza, A., Milanowski, B., Drużbicki, K., Jenczyk, J., Jarek, M., Mielcarek, J., Lulek, J., Pajzderska, A., & Wąsicki, J. (2017). *Molecular dynamics and the dissolution rate of nifedipine encapsulated in mesoporous silica.* https://doi.org/10.1016/J.MICROMESO.2017.05.019.

Letchmanan, K., Shen, S.-.C., Ng, W.K., Tan, R.B.H., 2015. Enhanced dissolution and stability of artemisinin by nano-confinement in ordered mesoporous SBA-15 particles. J. Microencapsul. 32 (4), 390–400. https://doi.org/10.3109/02652048.2015.1035684.

Li, F., Song, S., Guo, Y., Zhao, Q., Zhang, X., Pan, W., Yang, X., 2015. Preparation and pharmacokinetics evaluation of oral self-emulsifying system for poorly water-soluble drug Lornoxicam. Drug Deliv. 22 (4), 487–498. https://doi.org/10.3109/10717544.2014.885615.

Makrocka-Rydzyk, M., Woźniak-Braszak, A., Jurga, K., Jurga, S., 2015. Local motions in poly(ethylene-co-norbornene) studied by (1)H NMR relaxometry. Solid State Nucl. Magn. Reson. https://doi.org/10.1016/j.ssnmr.2015.08.005.

Meynen, V., Cool, P., Vansant, E.F., 2009. Verified syntheses of mesoporous materials. Microporous Mesoporous Mater. 125 (3), 170–223. https://doi.org/10.1016/j.micromeso.2009.03.046.

Moritz, M., Geszke-Moritz, M., 2015. Mesoporous materials as multifunctional tools in biosciences: principles and applications. Mater. Sci. Eng. C Mater. Biol. Appl. 49, 114–151. https://doi.org/10.1016/j.msec.2014.12.079.

Moutasim, M.Y., ElMeshad, A.N., El-Nabarawi, M.A., 2017. A pharmaceutical study on lornoxicam fast disintegrating tablets: formulation and in vitro and in vivo evaluation. Drug Deliv. Transl. Res. 7 (3), 450–459. https://doi.org/10.1007/s13346-017-0367-6.

Nijhawan, M., Santhosh, A., Babu, P.R.S., Subrahmanyam, C.V.S., 2014. Solid state manipulation of lornoxicam for cocrystals—Physicochemical characterization. Drug Dev. Ind. Pharm. 40 (9), 1163–1172. https://doi.org/10.3109/03639045.2013.804834.

Pardhi, V., Chavan, R.B., Thipparaboina, R., Thatikonda, S., Naidu, V., Shastri, N.R., 2017. Preparation, characterization, and cytotoxicity studies of niclosamide loaded mesoporous drug delivery systems. Int. J. Pharm. 528 (1–2), 202–214. https://doi.org/10.1016/j.ijpharm.2017.06.007.

Perego, C., Millini, R., 2013. Porous materials in catalysis: challenges for mesoporous materials. Chem. Soc. Rev. 42 (9), 3956–3976. https://doi.org/10.1039/c2cs35244c.

Sarkar, A., Ghosh, S., Chowdhury, S., Pandey, B., Sil, P.C., 2016. Targeted delivery of quercetin loaded mesoporous silica nanoparticles to the breast cancer cells. Biochim. Biophys. Acta 1860 (10), 2065–2075. https://doi.org/10.1016/j.bbagen.2016.07.001.

Slichter, C.P., 1990. Principles of Magnetic Resonance, 3rd ed. Springer-Verlag. https://doi.org/10.1007/978-3-662-09441-9.

Song, S.-.W., Hidajat, K., Kawi, S., 2005. Functionalized SBA-15 materials as carriers for controlled drug delivery: influence of surface properties on matrix-drug interactions. Langmuir: ACS J. Surfaces Colloids 21 (21), 9568–9575. https://doi.org/10.1021/la051167e.

Tawfeek, H.M., Saleem, I.Y., Roberts, M., 2014. Dissolution enhancement and formulation of rapid-release lornoxicam mini-tablets. J. Pharm. Sci. 103 (8), 2470–2483. https://doi.org/10.1002/jps.24073.

N. Thahir, R., Wahab, W., Nafie, A.L., Raya, I, 2019. Synthesis of mesoporous silica sba-15 through surfactant set-up and hydrothermal process Rasayan J. Chem. 12 (03), 1117–1126. https://doi.org/10.31788/RJC.2019.1235306.

Vishal, P., 2015. Fabrication and Characterization of Hexagonal Mesoporous Silica (HMS) for Impregnating Lornoxicam as a Drug Carrier. Austin Therapeutics 2, 1–5.

Wan, H., Liu, L., Li, C., Xue, X., Liang, X., 2009. Facile synthesis of mesoporous SBA-15 silica spheres and its application for high-performance liquid chromatography. J. Colloid Interface Sci. 337 (2), 420–426. https://doi.org/10.1016/j.jcis.2009.05.065.

Wang, Y., Sun, L., Jiang, T., Zhang, J., Zhang, C., Sun, C., Deng, Y., Sun, J., Wang, S., 2014. The investigation of MCM-48-type and MCM-41-type mesoporous silica as oral solid dispersion carriers for water insoluble cilostazol. Drug Dev. Ind. Pharm. 40 (6), 819–828. https://doi.org/10.3109/03639045.2013.788013.

Woźniak-Braszak, A., Knitter, M., Markiewicz, E., Ingram, W.F., Spontak, R.J., 2019. Effect of composition on the molecular dynamics of biodegradable isotactic polypropylene/thermoplastic starch blends. ACS Sustain. Chem. Eng. 7 (19), 16050–16059. https://doi.org/10.1021/acssuschemeng.9b02774.

Zhang, J., Tan, X., Gao, J., Fan, W., Gao, Y., Qian, S., 2013. Characterization of two polymorphs of lornoxicam. J. Pharm. Pharmacol. 65 (1), 44–52. https://doi.org/10.1111/j.2042-7158.2012.01573.x.

Zhao, D., Huo, Q., Feng, J., Chmelka, B.F., Stucky, G.D., 1998. Nonionic triblock and star diblock copolymer and oligomeric surfactant syntheses of highly ordered, hydrothermally stable, mesoporous silica structures. J. Am. Chem. Soc. 120 (24), 6024–6036. https://doi.org/10.1021/ja974025i.

Zhou, Y., Quan, G., Wu, Q., Zhang, X., Niu, B., Wu, B., Huang, Y., Pan, X., Wu, C., 2018. Mesoporous silica nanoparticles for drug and gene delivery. Acta Pharm. Sin. B 8 (2), 165–177. https://doi.org/10.1016/j.apsb.2018.01.007.